

Coherent potential approximation of random nearly isostatic kagome lattice

Xiaoming Mao¹ and T. C. Lubensky¹

¹*Department of Physics and Astronomy, University of Pennsylvania, Philadelphia, PA 19104, USA*

(Dated: August 13, 2010)

The kagome lattice has coordination number 4, and it is mechanically isostatic when nearest neighbor (NN) sites are connected by central force springs. A lattice of N sites has $O(\sqrt{N})$ zero-frequency floppy modes that convert to finite-frequency anomalous modes when next-nearest-neighbor (NNN) springs are added. We use the coherent potential approximation (CPA) to study the mode structure and mechanical properties of the kagome lattice in which NNN springs with spring constant κ are added with probability $\mathcal{P} = \Delta z/4$, where $\Delta z = z - 4$ and z is the average coordination number. The effective medium static NNN spring constant κ_m scales as \mathcal{P}^2 for $\mathcal{P} \ll \kappa$ and as \mathcal{P} for $\mathcal{P} \gg \kappa$, yielding a frequency scale $\omega^* \sim \Delta z$ and a length scale $l^* \sim (\Delta z)^{-1}$. To a very good approximation at small nonzero frequency, $\kappa_m(\mathcal{P}, \omega)/\kappa_m(\mathcal{P}, 0)$ is a scaling function of ω/ω^* . The Ioffe-Regel limit beyond which plane-wave states becomes ill-defined is reached at a frequency of order ω^* .

PACS numbers: 61.43.-j, 62.20.de, 46.65.+g, 05.70.Jk

I. INTRODUCTION

Understanding the nature of mechanical stability, how it arises, and how it can be controlled is important to fields ranging from civil engineering to biology. James Clerk Maxwell was among the first to address this problem with mathematical rigor in his 1864 paper [1] in which he established the conditions for the mechanical stability of a frame of points connected by lines or struts of fixed length. His approach, which can easily be generalized to treat particles interacting via central-force potentials or bonds between particles interacting via an angular potential, has since been used to study network glasses [2–4], randomly packed spheres near jamming [5, 6], networks of semi-flexible polymers [7, 8], regular [9] and random [10] periodic lattices, and a host of engineering problems [11, 12]. In this paper, we study the mode structure of a particular lattice - the kagome lattice shown in Fig. 1 - in which nearest neighbor (NN) sites are connected by harmonic central-force springs of spring constant k and next-nearest-neighbor (NNN) sites are randomly connected by similar springs but with a different spring constant κ . In the absence of NNN springs, finite realizations of this lattice are just on the verge of mechanical stability in the Maxwell sense. The addition of NNN springs renders the system stable. When these springs are added uniformly with a spring constant κ that is allowed to approach zero continuously [9, 13], the result is a kind of critical point at $\kappa = 0$ with a rich mode structure and diverging length and vanishing frequency scales as $\kappa \rightarrow 0$ that have direct counterparts in the properties of randomly packed spheres near jamming [14]. Here we use the coherent potential approximation or CPA [15, 16] (otherwise known as the effective medium approximation) to explore in detail the static and dynamical mechanical properties and mode structure of the kagome lattice as a function of the probability \mathcal{P} that NNN sites are connected by springs. We find that the effective medium NNN spring constant $\kappa_m(\mathcal{P}, \omega)$ scales as \mathcal{P}^2 for small \mathcal{P} , and it gives rise to length and frequency scales $l^* \sim \mathcal{P}^{-1}$

and $\omega^* \sim \mathcal{P}$. Beyond a characteristic frequency $\omega_D^* \sim \mathcal{P}$, the imaginary part of κ_m rises quickly and phonons scatter strongly. The Ioffe-Regel limit beyond which certain plane wave states become ill-defined is reached at a frequency slightly larger than ω_D^* .

A. Mechanical Stability and Floppy Modes

Maxwell [1] argued that each constraint in a system of N points in d -dimensions reduces the number, dN , of zero frequency modes of free points by one. Thus, the number of zero frequency modes in a system with N_c constraints is $N_0 = dN - N_c$. Of these, $d(d+1)/2$ are those of rigid translations and rotations, leaving $N_f = dN - N_c - d(d+1)/2$ internal zero frequency modes, which are usually referred to as floppy modes [3] or mechanisms in the engineering literature [12], when $dN - N_c - d(d+1)/2 \geq 0$. Mechanical stability requires that there be no floppy modes, or equivalently that $dN - N_c - d(d+1)/2 \leq 0$. Though Maxwell considered general frames of points, his analysis can immediately be applied to the determination of mechanical stability of extended crystals and glasses - as was first done in the context of network glasses, which are unstable in the absence of bending forces, by Phillips and Thorpe [2, 17] - in which points are replaced by particles or atoms and struts are replaced by inter-particle potentials.

If each particle in an extended system is on average connected by central-force potential creating bonds to z other particles, then, because each bond is shared by two particles, the system experiences $zN/2$ constraints if bond lengths are restricted to be at their equilibrium length and there are no redundant bonds [18], and it has $N_f = dN - \frac{1}{2}zN - \frac{1}{2}d(d+1)$ floppy modes. Thus, in the limit of large N , a central-force system is mechanically stable if $z > z_c = 2d$. In an infinitely extended system, z is independent of N . In a finite system cut from an infinite one, particles at the boundary have fewer neighbors than those in the interior, and z (which is an average

quantity) is of order $N^{-1/d}$ smaller than it would be in the ideal infinite system. Systems with $z = z_c$ are called isostatic. A finite piece of N particles cut from an infinite isostatic has a surface with of order $N^{(d-1)/d}$ cut bonds, and thus that many fewer constraints and that many more floppy modes. These modes generally remain floppy even if they have finite amplitudes if there are free boundary conditions. Because of their geometry with straight segments extending throughout their interior, the square, the kagome, and related lattice of N sites with periodic rather than free boundary conditions have $N^{(d-1)/d}$ infinitesimal floppy modes - modes that have zero energy for infinitesimal displacements but finite energy for large displacements [12]. The simplest example of an infinitesimal floppy modes is that of a mass connected to two identical co-linear springs that are rigidly attached to walls on either side of the mass. If the springs are not under tension, infinitesimal displacements of the particle perpendicular to the spring cost no energy but finite displacements do. Thus the harmonic kagome lattice has \sqrt{N} floppy modes.

The recently most explored random isostatic system is perhaps the system of randomly close-packed spheres at the jamming transition [14] in the system of frictionless soft spheres with one-sided repulsion. This transition occurs when the volume fraction ϕ of spheres just exceeds the critical value ϕ_c at which they form just enough contacts to support a compressional load. Thus at ϕ_c , the bulk modulus B jumps discontinuously to a nonzero value, the number of neighbors per particle grows as $\Delta z = z - z_c = (\phi - \phi_c)^{1/2}$, and the shear modulus grows continuously from zero as $G \sim (\phi - \phi_c)^{1/2} \sim (\Delta z)^1$. Associated with this transition are a diverging length scale $l^* \sim (\Delta z)^{-1}$ and vanishing frequency scale $\omega^* \sim \Delta z$ whose behavior follows from quite general “cutting” arguments [5].

B. Periodic Isostatic Lattices

Isostaticity is not limited to random systems. There are a number of periodic isostatic lattices with $z_{NN} = z_c$ NN bonds per particle. These include the hypercubic lattice in d dimensions and the kagome lattice in two-dimensions and its generalization to higher dimensions with NN bonds occupied by springs of spring constant k , all with $z = 2d$. They can be moved off isostaticity by introducing springs of spring constant κ on NNN bonds either homogeneously or randomly.

In homogeneous systems, the isostatic limit is continuously approached by allowing $\kappa \rightarrow 0$. In the square-lattice version of this model [9], the bulk modulus is nonzero at $\kappa = 0$, but the shear modulus vanishes as κ in this limit. In the kagome version, both the shear and the bulk moduli are nonzero at $\kappa = 0$. In both models, as in the jamming problem, there is a divergent length scale, $l^* \sim \kappa^{-1/2}$ and a vanishing frequency scale $\omega^* \sim \kappa^{1/2}$.

The Coherent Potential, or equivalently the effective

medium, Approximation (CPA) [15, 19–21] is a powerful tool for the calculation of properties of random systems, from the electronic structure of alloys [15, 22] to the elasticity of composite materials [23–25]. It has been used with great success in the study of rigidity percolation problem [16, 26, 27] and, more recently, in the dynamics of off-lattice systems near a rigidity threshold [28]. It also provides a quantitative theory of the static and dynamic phonon response in the nearly isostatic square lattice in which next-nearest-neighbor springs (NNN) are randomly added to a lattice in which all nearest-neighbor-site connected by equivalent springs [10]. In this lattice, the effective-medium NNN spring constant $\kappa_m(\mathcal{P}, \omega)$ has a zero-frequency limit, $\kappa_m(\mathcal{P}, 0)$, that scales as $\mathcal{P}^2 \sim (\Delta z)^2$ leading to lengths and frequencies that scale as $l^* \sim (\Delta z)^{-1}$ and $\omega^* \sim (\Delta z)^1$ as they do in the jamming problem. The finite-frequency spring constant is a scaling function of ω/ω^* at small \mathcal{P} : $\kappa_m(\mathcal{P}, \omega) = \kappa_m(\mathcal{P}, 0)h(\omega/\omega^*)$. As \mathcal{P} is increased, there is a crossover from nonaffine response at small \mathcal{P} to affine response with $\kappa_m(\mathcal{P}, 0) = \mathcal{P}\kappa$ at larger \mathcal{P} , much as there is in networks of semi-flexible polymers as the average polymer length is increased [29, 30]

C. Review of Results

In this paper, we use the CPA to explore in detail the static and dynamic properties of the kagome lattice as it is moved away from isostaticity by the random addition of NNN springs. Our approach is identical to that employed in our treatment of the square lattice [10], but calculations are considerably more complicated because each unit cell has three sites rather than a single one. The results of our calculations follow what we expect from our experience with the homogeneous square and kagome lattices and with the random square lattice. The bulk and shear moduli are nonzero and proportional to the NN spring constant k when $\mathcal{P} \rightarrow 0$. The static NNN effective medium spring constant $\kappa_m(\mathcal{P}, 0)$ scales as \mathcal{P}^2 leading to $l^* \sim (\Delta z)^{-1}$ and $\omega^* \sim (\Delta z)$ in agreement with cutting arguments. As is the case in the square lattice, $\kappa_m(\mathcal{P}, \omega)/\kappa_m(\mathcal{P}, 0)$ is a basically a scaling function of ω/ω^* at small \mathcal{P} , but with small yet important deviations at small ω that describe Rayleigh scattering, i.e., a mean-free-path that scales as ω^{-3} in $2d$.

The outline of this paper is as follows. In Sec. II we review the elasticity of the homogeneous nearly isostatic kagome lattice. In Sec. III we discuss the CPA on random nearly isotropic kagome lattice with the NNN bonds randomly occupied with probability \mathcal{P} . In Sec. IV we discuss the results of the CPA calculation, including the crossover of κ_m from \mathcal{P}^2 to \mathcal{P} behavior as \mathcal{P} increase or κ decreases, and the rapid increase of scattering at the characteristic frequency $\omega_D^* \sim \Delta z$.

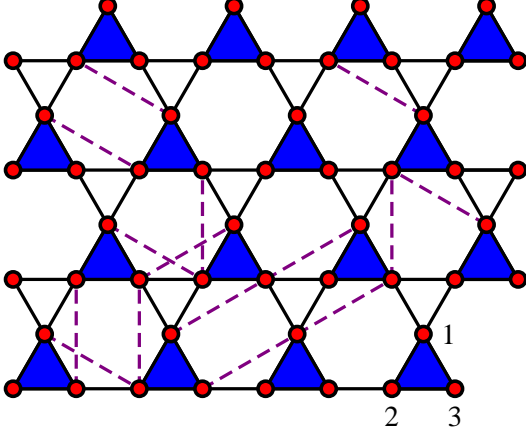


FIG. 1: The kagome lattice with random additional NNN bonds denoted by purple dashed lines. The unit cell triangle is marked with filled triangles. Particle 1, 2, 3 in each unit cell are marked in the bottom right unit cell.

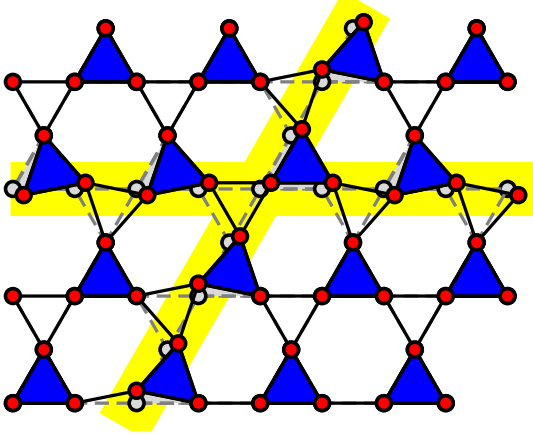


FIG. 2: The kagome lattice and its floppy modes, with the reference state in gray and deformed state in red. Two of its floppy modes are shown in this figure marked by the yellow ribbons.

II. HOMOGENEOUS NEARLY ISOSTATIC KAGOME LATTICE AND ITS ELASTICITY

A. Expansion of elastic energy in general lattice models

In this section we briefly review the elastic energy in central-force network models, in which the elastic energy U can be written as a sum of the energy of each central-force bond

$$U = \sum_b U_b(R_b), \quad (1)$$

where R_b is the length of the bond and U_b is the potential energy of the bond as a function of the length. We consider a displacement field on the network that maps particle ℓ which is at position $\mathbf{R}_{\ell 0}$ to a new posi-

tion $\mathbf{R}_\ell = \mathbf{R}_{\ell 0} + \mathbf{u}_\ell$, thus the length of bond b between particle ℓ and ℓ' is changed into

$$R_b = |\mathbf{R}_{\ell'} - \mathbf{R}_\ell|. \quad (2)$$

We refer to the original space in which particle ℓ is at $\mathbf{R}_{\ell 0}$ as the *reference space*, and the space after applying the displacement field as the *target space*. We consider harmonic potentials

$$U_b = \frac{k_b}{2}(R_b - R_{bR})^2, \quad (3)$$

where R_{bR} is the rest length of the bond, and k_b is the spring constant. The length R_b can be expanded for small displacement \mathbf{u} as

$$R_b = R_{b0} + \mathbf{e}_{b0} \cdot \mathbf{u}_b + \frac{1}{2R_{b0}} \mathbf{u}_b \cdot (\mathbf{I} - \mathbf{e}_{b0} \mathbf{e}_{b0}) \cdot \mathbf{u}_b + O(\mathbf{u}_b^3), \quad (4)$$

where $R_{b0} = |\mathbf{R}_{\ell'0} - \mathbf{R}_{\ell 0}|$, $\mathbf{u}_b = \mathbf{u}_{\ell'} - \mathbf{u}_\ell$, and $\mathbf{e}_{b0} = (\mathbf{R}_{\ell'0} - \mathbf{R}_{\ell 0})/|\mathbf{R}_{\ell'0} - \mathbf{R}_{\ell 0}|$ is the unit vector pointing along the bond in the reference space. Thus we have

$$U_b = \frac{k_b}{2}(R_{b0} - R_{bR})^2 + f_b \mathbf{e}_{b0} \cdot \mathbf{u}_b + \frac{1}{2} \mathbf{u}_b \cdot \left[k_b \mathbf{e}_{b0} \mathbf{e}_{b0} + \frac{f_b}{R_{b0}} (\mathbf{I} - \mathbf{e}_{b0} \mathbf{e}_{b0}) \right] \cdot \mathbf{u}_b, \quad (5)$$

where $f_b = U'_b(R) = k_b(R_{b0} - R_{bR})$ is the magnitude of the force on the bond in the reference space. In general we consider the case in which the reference state is in mechanical equilibrium, which means that the total force on each particle vanishes

$$\mathbf{f}_\ell = \sum_{b(\ell, \ell')} f_b \mathbf{e}_{b0} = 0 \quad (6)$$

where the sum $\sum_{b(\ell, \ell')}$ is over all occupied bonds connected to ℓ . However, to capture the properties of random networks, which often carry residual stress, the length of each bond is not necessarily at its rest length, i.e., $R_{b0} - R_{bR} \neq 0$ in general.

The change of the elastic energy from the reference space to the target space of the whole system is then a quadratic form of the displacement field

$$\Delta U = \sum_b \frac{1}{2} \mathbf{u}_b \cdot \left[k_b \mathbf{e}_{b0} \mathbf{e}_{b0} + \frac{f_b}{R_{b0}} (\mathbf{I} - \mathbf{e}_{b0} \mathbf{e}_{b0}) \right] \cdot \mathbf{u}_b, \quad (7)$$

which can also be written as

$$\Delta U = \sum_b \frac{1}{2} \left[k_b (\mathbf{u}_b^\parallel)^2 + \frac{f_b}{R_{b0}} (\mathbf{u}_b^\perp)^2 \right], \quad (8)$$

where \mathbf{u}_b^\parallel is the component of \mathbf{u}_b parallel to \mathbf{e}_{b0} and \mathbf{u}_b^\perp is the component perpendicular to \mathbf{e}_{b0} .

By doing a gradient expansion on the displacement field,

$$\mathbf{u}_b = R_{b0} \mathbf{e}_{b0k} \partial_k \mathbf{u}(\mathbf{r}), \quad (9)$$

where $\mathbf{u}(\mathbf{r})$ is the displacement field at position \mathbf{r} , we recover the elastic energy of the continuum theory

$$\Delta U = \int d\mathbf{r} K_{ijkl} \partial_k u_i \partial_l u_j, \quad (10)$$

with

$$K_{ijkl} = \sum_{\mathbf{b}} \frac{R_{b0}^2}{2v_0} e_{b0k} e_{b0l} \cdot \left[k_b e_{b0i} e_{b0j} + \frac{f_b}{R_{b0}} (\delta_{ij} - e_{b0i} e_{b0j}) \right] \quad (11)$$

where the summation $\sum_{\mathbf{b}}$ is over bonds connecting to one particle, and we are using a simple lattice with one particle per unit cell in this illustration. The volume of a unit cell is denoted by v_0 .

B. Elastic energy of the kagome lattice

The kagome lattice is a lattice with three particles per unit cell, and we shall use the following displacement vector to denote the deformation of the lattice

$$\mathbf{u}_\ell = (u_{\ell,1,x}, u_{\ell,1,y}, u_{\ell,2,x}, u_{\ell,2,y}, u_{\ell,3,x}, u_{\ell,3,y}), \quad (12)$$

where ℓ labels the unit cell and $(1, 2, 3)$ label the particles in the unit cell as in Fig. 2. As we have discussed, the elastic energy can be expanded in small displacement field \mathbf{u} , and to leading order we have the quadratic form

$$\Delta U = \frac{1}{2} \sum_{\ell, \ell'} \mathbf{u}_\ell \cdot \mathbf{D}_{\ell, \ell'} \cdot \mathbf{u}_{\ell'}, \quad (13)$$

which can be built from the analysis as in Eq. (7), but generalized to the case of the kagome lattice which has three sites per unit cell. The matrix \mathbf{D} is called the dynamical matrix of the lattice. This elastic energy can be written in momentum space as

$$\Delta U = \frac{1}{2N^2} \sum_{\mathbf{q}, \mathbf{q}'} \mathbf{u}_{\mathbf{q}} \cdot \mathbf{D}_{-\mathbf{q}, \mathbf{q}'} \cdot \mathbf{u}_{\mathbf{q}'}, \quad (14)$$

where the Fourier transform into momentum space is defined as

$$\begin{aligned} \mathbf{u}_{\mathbf{q}} &= \sum_{\ell} \mathbf{u}_\ell e^{-i\mathbf{q} \cdot \mathbf{R}_{\ell 0}} \\ \mathbf{u}_\ell &= \frac{1}{N} \sum_{\mathbf{q}} \mathbf{u}_{\mathbf{q}} e^{i\mathbf{q} \cdot \mathbf{R}_{\ell 0}}, \end{aligned} \quad (15)$$

where N is the number of unit cells. The dynamical matrix for the homogeneous kagome lattice with all NN bonds occupied with springs of spring constant k and all NNN bonds with springs of spring constant κ is a 6×6 matrix given by

$$\begin{aligned} \mathbf{D}_{\mathbf{q}, \mathbf{q}'} &= N \delta_{\mathbf{q}, \mathbf{q}'} \mathbf{D}_{\mathbf{q}}(k, \kappa) \\ \mathbf{D}_{\mathbf{q}}(k, \kappa) &= k \sum_{m \in NN} \mathbf{B}_{m, \mathbf{q}}^{NN} \mathbf{B}_{m, -\mathbf{q}}^{NN} \\ &\quad + \kappa \sum_{m \in NNN} \mathbf{B}_{m, \mathbf{q}}^{NNN} \mathbf{B}_{m, -\mathbf{q}}^{NNN}, \end{aligned} \quad (16)$$

where the \mathbf{B} vectors and their derivation are given in App. A.

C. The homogeneous kagome lattice and its low energy theory

There are six translational degrees of freedom per unit cell in the kagome lattice giving rise to six phonon branches. Of these, three are optical branches with frequencies of order \sqrt{k} , two are acoustic branches with sound velocities of order \sqrt{k} , and one is the anomalous branch. The later three branches, which determines the low-energy elastic theory of the kagome lattice, have modes in the space spanned by the following three vectors

$$\begin{aligned} \nu_1 &= (1/\sqrt{3})(1, 0, 1, 0, 1, 0) \\ \nu_2 &= (1/\sqrt{3})(0, 1, 0, 1, 0, 1) \\ \nu_3 &= \left(-\frac{1}{\sqrt{3}}, 0, \frac{1}{2\sqrt{3}}, -\frac{1}{2}, \frac{1}{2\sqrt{3}}, \frac{1}{2}\right), \end{aligned} \quad (17)$$

which correspond to two translations of the whole unit cell in x and y directions and the rotation of the unit-cell triangle around its center. The low-energy theory is governed by the 3×3 reduced dynamical matrix obtained by integrating out the three high-energy optical branches, as shown in App. B 1.

For small momentum, $|\mathbf{q}| < q_H^* = 4\sqrt{3\kappa/k}$, the reduced dynamical matrix is simply diagonalized by longitudinal and transverse acoustic phonons (which are linear combinations of ν_1 and ν_2) with speeds of sound $c_L = \sqrt{3k}/4$ and $c_T = \sqrt{k}/4$ and the rotational mode with a characteristic frequency $\omega_O^* = \sqrt{6\kappa}$ at $\mathbf{q} = 0$. The bulk modulus B and the shear modulus G are related, respectively, to the longitudinal and transverse sound velocities through

$$c_L^2 = (B + G)/\varrho; \quad c_T^2 = G/\varrho, \quad (18)$$

where ϱ is the mass density, which because there are three atoms per unit cell, is equal to 3 in our units. Thus, $B = 3k/8$ and $G = 3k/16$. There is only weak mixing between the rotational modes and the acoustic phonons, and the system is isotropic.

For large momentum $|\mathbf{q}| > q_H^* = 4\sqrt{3\kappa/k}$, strong mixing between the transverse acoustic modes and the rotational modes occurs, and the strong anisotropy of the isostatic state is retrieved. The mixing is maximal along $q_x = 0$ and symmetry equivalent directions, which we refer to as the isostatic directions, and the resulting two modes are shown in Fig. 3. The anomalous branch, with frequency of order κ , is the lower branch of the two. In the limit of $\kappa = 0$, the lattice becomes isostatic, the isotropic region is squeezed to the origin, and the anomalous modes reduce to the isostatic floppy modes with zero frequency along $q_x = 0$ (ΓM line in Fig. 3) and symmetry equivalent directions as depicted in Fig. 2. The name ‘‘anomalous modes’’ follows the nomenclature of Ref. [6],

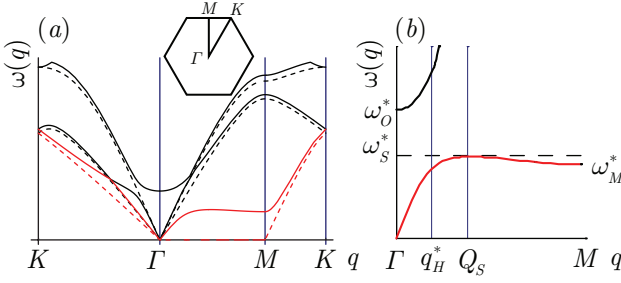


FIG. 3: (color online) (a) Phonon dispersion along symmetry directions. The dotted lines are for $\kappa = 0$ and the solid lines are for $\kappa = 0.02$. The floppy and anomalous branches are in red. (b) shows anomalous and shear modes along ΓM and indicates characteristic frequencies and wavenumbers. Frequencies ω_O^* , ω_S^* and ω_M^* are defined in the text. (From Ref. [9])

referring to the modes developed from the floppy modes as the system is moved away from the isostatic point. For a more detailed discussion of the low energy theory of the elasticity of the kagome lattice, see App. B 1.

Of particular interest is the frequency of the anomalous modes in the vicinity of $q_x = 0$. The squared frequency of these modes can be written as

$$\omega^2(\mathbf{q}) = \omega_A^2(q_y) + c_x^2 q_x^2, \quad (19)$$

where $c_x = c_L = \sqrt{3k}/4$. The function $\omega_A^2(q_y)$ is plotted in Fig. 4. It reaches a maximum value of $(\omega_S^*)^2$ at a $2d$ saddle point at $q_y = Q_S$ and a local minimum value of $(\omega_M^*)^2$ at the zone edge $q_y = Q_M = 2\pi/\sqrt{3}$. For small κ , $Q_S \simeq 4(3\kappa/2k)^{1/4}$, $(\omega_S^*)^2 \simeq 3\kappa$ and $(\omega_M^*)^2 \simeq 2\kappa$. All of the characteristic frequencies $\omega_O^* > \omega_S^* > \omega_M^*$ are proportional to $\sqrt{\kappa}$ for small κ . $\omega_A^2(q_y)$ is well approximated between $q_y = Q_S$ and $q_y = Q_M$ by

$$\omega_A^2 \approx \frac{1}{Q_M - Q_S} [Q_M \omega_S^2 - Q_S \omega_M^2 - q_y (\omega_S^2 - \omega_M^2)], \quad (20)$$

as is evident from Fig. 4. This relation will prove useful in our evaluation of integrals in our CPA analysis in Sec. III

Lengths scaling as $\kappa^{-1/2}$ can be extracted from the phonon dispersion relations in various ways. One length is the hybridization length l_H^* obtained from the hybridization wavenumber $q_H^* = 4\sqrt{3\kappa/k} = l_H^{*-1}$ separating the domain of predominantly transverse phonon behavior at low q_y from the domain of predominantly rotation behavior at high q_y . Other lengths can be obtained by comparing the $c_x q_x^2$ term in $\omega^2(\mathbf{q})$ to ω_M^2 and ω_S^2 : $q_M^* = \omega_M/c_x = l_m^{*-1} = (8/\sqrt{6})\sqrt{\kappa/k}$ and $q_S^* = \omega_S/c_x = l_s^{*-1} = 4\sqrt{\kappa/k}$. An interesting property of $\omega_A^2(q_y)$ is that the hybridization frequency ω_H^* obtained by setting $q_y = q_H^*$ in the transverse phonon frequency is identical to ω_S^* : $c_T q_H^* \equiv \omega_H^* = \omega_S^*$.

One experimentally relevant quantity is the Fourier transform of the finite temperature static phonon cor-

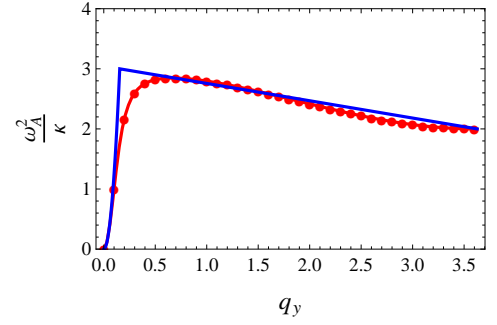


FIG. 4: (color online) Eigenvalue of the isostatic mode along isostatic directions, e.g., $q_x = 0$, for $\kappa = 5 \times 10^{-4}$. The eigenvalue of the full 6×6 dynamical matrix, ω^2 , normalized by κ , is denoted by the red dots, and the eigenvalue of the 3×3 reduced dynamical matrix (B2) is denoted by the red line. The blue line represents the approximation (20) we used in the asymptotic calculation in the f in CPA.

relation function $\mathcal{G}_{\mu,\nu}(\mathbf{l}, \mathbf{l}')$:

$$\mathcal{G}_{\mu,\nu}(\mathbf{q}) = k_B T \sum_{\alpha} \frac{e_{\mu}^{\alpha}(-\mathbf{q}) e_{\nu}^{\alpha}(\mathbf{q})}{\omega_{\alpha}^2(\mathbf{q})}, \quad (21)$$

where μ and ν label the basis defined in Eq. (12) of the 6-dimensional space of \mathbf{u} , α labels the phonon band, and $e_{\mu}^{\alpha}(\mathbf{q})$ is the 6-dimensional eigenvector associated with mode (α, \mathbf{q}) . This correlation function is in the zero-frequency limit and thus independent of dissipation of the system. The quantities $\omega_{\alpha}^2(\mathbf{q})$ are merely the eigenvalues of the dynamical matrix with the zero-frequency value of the spring constant (the effective medium spring constant can depend on frequency as we discuss below in the CPA). The diverging length scale $l^* \sim \kappa^{-1/2}$ can be extracted this way from the static phonon correlation function in experiments.

III. THE COHERENT POTENTIAL APPROXIMATION ON THE RANDOM NEARLY ISOSTATIC KAGOME LATTICE

The CPA is a widely used method in the study of disordered systems [15, 16, 27]. In it, a random system is mapped into an effective medium with no disorder that is described by a Green's function with a suitable self-energy that can capture the effect of the disorder average of the randomness. To achieve this, one imposes a self-consistency constraint that the effective medium Green's function perturbed by the presence of single impurity in the effective medium reduces to the effective medium Green's function when averaged over the probability distribution of the impurity. More specifically, the T -matrix of this perturbation vanishes upon averaging over configurations that contain and do not contain the impurity.

For the case of the nearly isostatic kagome lattice, the effective medium has all NNN bonds occupied with an

effective-medium spring of spring constant $\kappa_m(\mathcal{P}, \omega)$, and the effective medium Green's function is identical to that of a homogeneous system with $\kappa = \kappa_m(\mathcal{P}, \omega)$. The CPA procedure consists of replacing one arbitrary NNN bond with a new bond of spring constant κ_s , which takes on the value κ with probability \mathcal{P} (bond occupied) and the value 0 with probability $1 - \mathcal{P}$ (bond unoccupied). This procedure leads to a modified dynamical matrix

$$\mathbf{D}^V = \mathbf{D} + \mathbf{V}, \quad (22)$$

where

$$\mathbf{V}_{\mathbf{q}, \mathbf{q}'}(k, \kappa) = (\kappa_s - \kappa_m) \mathbf{B}_{1, \mathbf{q}}^{NNN} \mathbf{B}_{1, -\mathbf{q}'}^{NNN}, \quad (23)$$

where 1 represents the arbitrary NNN bond we have chosen to replace into κ_s . This form of \mathbf{V} follows directly from the calculations leading to Eq. (16). It depends on the wavenumbers \mathbf{q} and \mathbf{q}' because the perturbed system is not translationally invariant.

The phonon Green's function for the effective medium is

$$\mathbf{G}_{\mathbf{q}}(\omega) = [\omega^2 \mathbf{I} - \mathbf{D}_{\mathbf{q}}]^{-1}. \quad (24)$$

In the perturbed system with one bond replaced, the Green's function becomes

$$\mathbf{G}_{\mathbf{q}, \mathbf{q}'}^V(\omega) = [\omega^2 \mathbf{I} - \mathbf{D}^V]_{\mathbf{q}, \mathbf{q}'}^{-1} \quad (25)$$

and is no longer translationally invariant. This Green's function can be expanded for small \mathbf{V}

$$\begin{aligned} \mathbf{G}_{\mathbf{q}, \mathbf{q}'}^V &= (\mathbf{I} - \mathbf{G} \cdot \mathbf{V})_{\mathbf{q}, \mathbf{q}'}^{-1} \cdot \mathbf{G}_{\mathbf{q}'} \\ &\simeq N \delta_{\mathbf{q}, \mathbf{q}'} \mathbf{G}_{\mathbf{q}} + \mathbf{G}_{\mathbf{q}} \cdot \mathbf{V}_{\mathbf{q}, \mathbf{q}'} \cdot \mathbf{G}_{\mathbf{q}'} \\ &\quad + \frac{1}{N} \sum_{\mathbf{q}_1} \mathbf{G}_{\mathbf{q}} \cdot \mathbf{V}_{\mathbf{q}, \mathbf{q}_1} \cdot \mathbf{G}_{\mathbf{q}_1} \cdot \mathbf{V}_{\mathbf{q}_1, \mathbf{q}'} \cdot \mathbf{G}_{\mathbf{q}'} + \dots, \end{aligned} \quad (26)$$

where we have dropped the frequency ω dependence which is the same for every \mathbf{G} and \mathbf{V} . This series can be written as

$$\mathbf{G}_{\mathbf{q}, \mathbf{q}'}^V = N \delta_{\mathbf{q}, \mathbf{q}'} \mathbf{G}_{\mathbf{q}} + \mathbf{G}_{\mathbf{q}} \cdot \mathbf{T}_{\mathbf{q}, \mathbf{q}'} \cdot \mathbf{G}_{\mathbf{q}'}, \quad (27)$$

where

$$\begin{aligned} \mathbf{T}_{\mathbf{q}, \mathbf{q}'} &\equiv \mathbf{V}_{\mathbf{q}, \mathbf{q}'} + \frac{1}{N} \sum_{\mathbf{q}_1} \mathbf{V}_{\mathbf{q}, \mathbf{q}_1} \cdot \mathbf{G}_{\mathbf{q}_1} \cdot \mathbf{V}_{\mathbf{q}_1, \mathbf{q}'} \\ &\quad + \frac{1}{N^2} \sum_{\mathbf{q}_1, \mathbf{q}_2} \mathbf{V}_{\mathbf{q}, \mathbf{q}_1} \cdot \mathbf{G}_{\mathbf{q}_1} \cdot \mathbf{V}_{\mathbf{q}_1, \mathbf{q}_2} \cdot \mathbf{G}_{\mathbf{q}_2} \cdot \mathbf{V}_{\mathbf{q}_2, \mathbf{q}'} \\ &\quad + \dots, \end{aligned} \quad (28)$$

is the T -matrix expressed in the wavenumber basis.

In the CPA, the effective medium spring constant κ_m is determined by requiring that the average value of $\mathbf{G}_{\mathbf{q}, \mathbf{q}'}^V$ be equal to $N \delta_{\mathbf{q}, \mathbf{q}'} \mathbf{G}_{\mathbf{q}}$ or equivalently that the disorder average of the T -matrix vanish:

$$\mathcal{P} \mathbf{T}|_{\kappa_s = \kappa} + (1 - \mathcal{P}) \mathbf{T}|_{\kappa_s = 0} = 0. \quad (29)$$

The evaluation of the T -matrix is simplified by the following identity,

$$\frac{1}{N} \sum_{\mathbf{q}_1} \mathbf{V}_{\mathbf{q}, \mathbf{q}_1} \cdot \mathbf{G}_{\mathbf{q}_1} \cdot \mathbf{V}_{\mathbf{q}_1, \mathbf{q}'} \quad (30)$$

$$\begin{aligned} &= (\kappa_s - \kappa_m)^2 \mathbf{B}_{1, \mathbf{q}}^{NNN} \\ &\quad \times \frac{1}{N} \left(\sum_{\mathbf{q}_1} \mathbf{B}_{1, -\mathbf{q}_1}^{NNN} \cdot \mathbf{G}_{\mathbf{q}_1} \cdot \mathbf{B}_{1, \mathbf{q}}^{NNN} \right) \mathbf{B}_{1, -\mathbf{q}'}^{NNN} \end{aligned} \quad (31)$$

$$= -(\kappa_s - \kappa_m) \mathbf{V}_{\mathbf{q}, \mathbf{q}'} f(\kappa_m, \omega), \quad (32)$$

where

$$f(\kappa_m, \omega) = -v_0 \int_{1BZ} \frac{d^2 \mathbf{q}}{4\pi^2} \mathbf{B}_{1, -\mathbf{q}}^{NNN} \cdot \mathbf{G}_{\mathbf{q}}(\omega) \cdot \mathbf{B}_{1, \mathbf{q}}^{NNN}, \quad (33)$$

with $v_0 = \sqrt{3}/2$ the area of the unit cell in real space and $4\pi^2/v_0 = 8\pi^2/\sqrt{3}$ is the area of the first Brillouin zone in reciprocal space. The integral is over the first Brillouin zone. The Green's function $\mathbf{G}_{\mathbf{q}}(\omega)$ is the phonon Green's function in the effective medium so it depends on κ_m . Using these relations in Eq. (28) gives

$$\mathbf{T}_{\mathbf{q}, \mathbf{q}'} = \frac{\mathbf{V}_{\mathbf{q}, \mathbf{q}'}}{1 + (\kappa_s - \kappa_m) f(\kappa_m, \omega)}. \quad (34)$$

Thus, the self-consistency equation (29) requires that

$$f(\kappa_m, \omega) \kappa_m^2 - (1 + \kappa f(\kappa_m, \omega)) \kappa_m + \mathcal{P} \kappa = 0, \quad (35)$$

from which one can solve for the effective medium NNN spring constant κ_m for any given \mathcal{P} and ω . The form of this solution at small κ_m depends on the behavior of the function $f(\kappa_m, \omega)$ at small κ_m , which is in turn determined by the form of the anomalous mode along the $q_x = 0$ and other isostatic directions. Details of the calculation of $f(\kappa_m, \omega)$ are presented in App. B.

In the following discussion unless otherwise stated, we use reduced units with $k = 1$ and lattice constant $a = 1$, and thus unitless spring constants, and elastic moduli, and frequencies: $\kappa/k \rightarrow \kappa$, $Ga^2/k \rightarrow G$, and $\omega/\sqrt{k} \rightarrow \omega$.

IV. RESULTS AND DISCUSSION

A. CPA solution at zero frequency: static response

We first consider the case of $\omega = 0$, which characterizes the static response of the system. For small \mathcal{P} , we expect that the effective medium spring constant κ_m also to be small and that we can, therefore, ignore the $f(\kappa_m, \omega) \kappa_m^2$ term in the CPA self-consistency equation (35). Using the asymptotic small κ_m limit $f(\kappa_m, 0) = \mathcal{B}/\sqrt{\kappa_m}$, where $\mathcal{B} = 5(1 - \sqrt{2/3})$, derived in App. B [Eq. (B13)], we obtain the equation for κ_m at small \mathcal{P}

$$\kappa_m + \mathcal{B} \kappa \sqrt{\kappa_m} - \mathcal{P} \kappa = 0, \quad (36)$$

which has the solution

$$\kappa_m(\mathcal{P}, 0) = \left[\frac{-\mathcal{B}\kappa + \sqrt{\mathcal{B}^2\kappa^2 + 4\mathcal{P}\kappa}}{2} \right]^2. \quad (37)$$

This solution has two limits:

$$\kappa_m(\mathcal{P}, 0) \simeq \begin{cases} \mathcal{A}\mathcal{P}^2 & \text{if } \mathcal{P} \ll (\mathcal{B}^2/4)\kappa, \\ \mathcal{P}\kappa & \text{if } \mathcal{P} \gg (\mathcal{B}^2/4)\kappa, \end{cases} \quad (38)$$

where $\mathcal{A} = 1/\mathcal{B}^2 = 3(5 + 2\sqrt{6})/25$. In the first case, $\kappa\sqrt{\kappa_m} \gg \kappa_m$, and the solution for κ_m is obtained by ignoring the first term in Eq. (36); in the second case, the opposite is true, and κ_m is obtained by ignoring the second term in this equation. In the second case, every *NNN* bond distorts in the same way under stress, and response is affine. In the first case $\kappa_m = \mathcal{A}\mathcal{P}^2 \ll \mathcal{P}\kappa$, indicating that the response is nonaffine with local rearrangements in response to stress. Within the CPA, this result emerges because of the divergent elastic response encoded in \mathbf{G} (and $f(\kappa_m, 0)$) as $\kappa_m \rightarrow 0$ (See App. B). The nonaffine regime arises when *NNN* springs are strong enough for the second term in Eq. (36) to dominate the first. As κ approaches zero at fixed \mathcal{P} , distortions produced by the extra bond decrease and the nonaffine regime becomes vanishingly small. Numerical solutions of the CPA self-consistency equation (35) with the full 6×6 dynamical matrix is plotted in Fig. 5, along with a comparison to the analytical solution (37) and the two asymptotic forms in Eq. (38).

This crossover of the effective medium spring constant κ_m between \mathcal{P}^2 and \mathcal{P} is different from the nonaffine-affine crossover in the case of random nearly isostatic square lattice [10] which describes the response of the square lattice to shear stress, because the shear modulus (more precisely, C_{44}) is proportional to the effective medium spring constant κ_m for the *NNN* bonds in the square lattice. In the case of kagome lattice in this Paper, the shear modulus is finite and proportional to k , whereas κ_m mainly determines the rigidity of the lattice with respect to the floppy mode, which are essentially rotations of the triangles as shown in Fig. 2.

Length and frequency scales can be extracted in the static limit much as they were extracted in the homogeneous case discussed in Sec. II. The finite temperature static phonon correlation function \mathcal{G} is the inverse of the dynamical matrix evaluated at $\omega = 0$, whose eigenvalues and eigenvectors are identical to those of the homogeneous case with κ replaced by $\kappa_m \equiv \kappa_m(\mathcal{P}, 0)$. The eigenvalues allows us to identify frequencies by taking the square roots of the appropriate eigenvalues of \mathbf{D} :

$$\omega_O^* = \sqrt{6\kappa_m} > \omega_S^* = \sqrt{3\kappa_m} > \omega_M^* = \sqrt{2\kappa_m}. \quad (39)$$

Unlike the situation homogeneous lattices, these frequencies are not equal to any physical dynamical-mode frequency of the system. They do, however, provide information about the static properties of the phonon correlation function \mathcal{G} that could in principle be measured

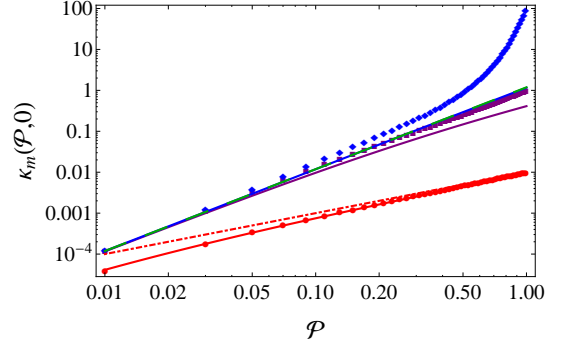


FIG. 5: (color online) CPA solution at zero frequency. Data points show the numerical solution κ_m as a function of \mathcal{P} at $\omega = 0$ of the CPA self-consistency equation (35) with the full 6×6 dynamical matrix. *NNN* bond spring constant $\kappa = 10^{-2}, 10^0, 10^2$ are shown in red dots, purple squares, and blue diamonds respectively. The analytical solution (37) of these three cases at small \mathcal{P} are shown in red, purple, and blue lines. Also shown are the nonaffine ($\kappa_m = \mathcal{A}\mathcal{P}^2$) and affine ($\kappa_m = \mathcal{P}\kappa$ at $\kappa = 10^{-2}$) limits in green dashed line and red dash-dotted line. At large \mathcal{P} the numerical solution, especially the one for $\kappa = 10^2$ deviate significantly from the nonaffine limit form because Eq. (36) is an approximation at small \mathcal{P} by ignoring the highest order term in Eq. (35).

at finite temperature via scattering or particle tracking experiment. They also lead to diverging lengths just as they do in the homogeneous case:

$$l^* \equiv l_H^* = \frac{1}{\sqrt{3}} l_S^* = \sqrt{2} l_M^* = \frac{1}{4\sqrt{3\kappa_m}} = \frac{1}{\sqrt{3\mathcal{A}}} \frac{1}{\Delta z} \quad (40)$$

B. CPA solution at finite frequency: dynamic response and damping

For finite frequency ω , the effective medium spring constant is complex, $\kappa_m(\mathcal{P}, \omega) = \kappa'_m(\mathcal{P}, \omega) - i\kappa''_m(\mathcal{P}, \omega)$, where the imaginary part $\kappa''_m(\mathcal{P}, \omega)$, which describes damping of phonons in this random network, is odd in ω and positive for $\omega > 0$. From the analysis for the static limit $\omega = 0$, we see that the interesting case is the nonaffine regime with $\mathcal{P} \ll (\mathcal{B}^2/4)\kappa$, in which the self-consistency equation (36) simplifies to

$$f(\kappa_m, \omega)\kappa_m = \mathcal{P}. \quad (41)$$

In the static limit, $f(\kappa_m, 0) \sim \kappa_m^{-1/2}$ is singular in the $\kappa_m \rightarrow 0$ limit. As we show in App. B, at finite frequency, $f(\kappa_m, \omega) \sim [\sqrt{(3\kappa_m - \omega^2)/\kappa_m} - \sqrt{(2\kappa_m - \omega^2)/\kappa_m}]/\kappa_m$, which leads to

$$\kappa_m(\mathcal{P}, \omega) = \frac{3\mathcal{P}^2}{25} \left(5 + 2\sqrt{6} \sqrt{1 - \frac{25\omega^2}{18\mathcal{P}^2}} \right), \quad (42)$$

as depicted in Fig. 6. Taking $\omega = 0$, this solution reduces to the zero-frequency solution [Eq. (38)] in the

nonaffine limit. Equation (42) develops an imaginary part when $|\omega| > 2\sqrt{3}\mathcal{P}/5$, which, as we discussed above must be negative for $\omega > 0$. It is straightforward to see that this solution satisfies the scaling form $\kappa_m(\mathcal{P}, \omega) = \kappa_m(\mathcal{P}, 0)h(\omega/\omega^*)$, as does the CPA effective NNN spring constant in the square lattice Ref. [10]. This solution shows a rapid increase of damping beyond a characteristic frequency

$$\omega_D^* = \frac{2\sqrt{3}\mathcal{P}}{5}, \quad (43)$$

marking another characteristic frequency that scales also as \mathcal{P} .

Numerical solution of the CPA self-consistency equation (35) using the full 6×6 dynamical matrix is also shown in Fig. 6. We see that the asymptotic form (42) captures the solution fairly well.

This special behavior of the imaginary part of the effective medium spring constant κ_m is related to the phonon spectrum of the kagome lattice. As we have discussed in Sec II, at low frequencies, there is only very weak mixing between the rotational branch which is strongly affected by the NNN bonds and the acoustic phonon branches which are only very weakly scattered by the NNN bonds, and thus the damping to the acoustic phonons is very weak. On the other hand, for higher frequencies the transverse phonon strongly mixes with the rotational modes, making the damping rapidly increase with scatterings from the NNN bonds beyond ω_D^* , although the exact value of ω_D^* may be an artifact of the CPA method. The weak scattering below ω_D^* is not captured by the asymptotic form (42) for small κ_m because the function $\kappa_m(\mathcal{P}, \omega)$ in Eq. (42) was obtained using the dominant small κ_m limit of the integral $f(\kappa_m, \omega)$. There are, however, contributions to this integral that do not diverge and that contribute a subdominant imaginary part to κ_m , even when $\omega < \omega_D^*$, that is of order $\mathcal{P}^3\omega^2$ at small ω corresponding to Rayleigh scattering. More discussion is included in App. B.

In the homogeneous case, the eigenvalues of the dynamical matrix lead naturally to the identification of characteristic frequencies ω_S^* , and ω_M^* that vanish as $\sqrt{\kappa}$ in the limit of $\kappa \rightarrow 0$. In the random case, we have to deal with both the frequency-dependence $\kappa_m(\mathcal{P}, \omega)$ and the fact that it is a complex number, and we must ask whether these frequencies have any real meaning. As discussed earlier in Sec. II C, we can extract frequencies from the static dynamical matrix in exactly the same way that we did for the homogeneous case, and they satisfy

$$\omega_O^* = 3.85\omega_D^* > \omega_S^* = 2.72\omega_D^* > \omega_M^* = 2.22\omega_D^* > \omega_D^*. \quad (44)$$

Thus all of these frequencies are greater than the frequency ω_D . As a result, the signatures in the phonon dispersion relation including the hybridization and the saddle point are washed out by the strong scattering, as is shown in Fig. 8.

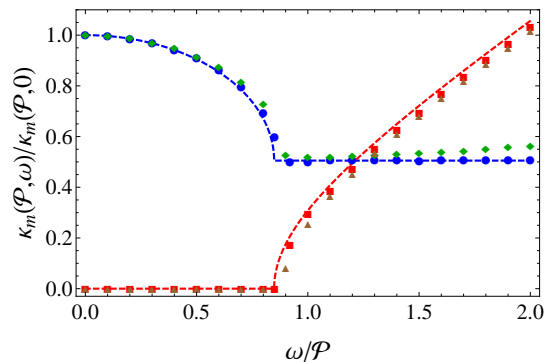


FIG. 6: (color online) CPA solution at finite frequency for $\mathcal{P} = 0.01$ and $\mathcal{P} = 0.05$. The numerical solution to Eq. (35) with the full 6×6 dynamical matrix is shown as the data points. Blue circles and red squares represent real and (negative of) imaginary parts of κ_m at $\mathcal{P} = 0.01$, and green diamonds and brown triangles represent the real and (negative of) imaginary parts of κ_m at $\mathcal{P} = 0.05$. The asymptotic form (42) is shown as the blue (real) and red (negative of imaginary) lines. In this plot frequency is rescaled by \mathcal{P} , and the effective medium spring constant κ_m is rescaled by its value at zero frequency which is real.

C. Phonon density of states

The phonon density of states (DOS) can be calculated from the retarded Green's function through

$$\rho(\omega) = -\frac{1}{\pi} \text{Tr} \text{Im} \mathbf{G}(\mathbf{q}, \omega) \quad (45)$$

where the trace is over both momentum \mathbf{q} and the phonon modes. Using this we get the phonon DOS of the effective medium solved from the CPA, as plotted in Fig. 7. As a comparison, we also show the phonon DOS of a periodic kagome lattice with the NNN spring constant equal to $\kappa_m(\mathcal{P}, 0)$, which is real valued.

For small frequencies, at which the imaginary part of the CPA solution $\kappa_m(\mathcal{P}, \omega)$ is very small, the two DOS are very close, and can be fitted nicely by the Debye-like total DOS of the transverse and the longitudinal phonons

$$\rho_s(\omega) = \frac{\omega}{(4\pi/\sqrt{3})c_L^2} + \frac{\omega}{(4\pi/\sqrt{3})c_T^2} \quad (46)$$

where $c_L^2 = 3k/16$ and $c_T^2 = k/16$ are respectively the longitudinal and transverse speed of sound (we have taken $k = 1$ as stated earlier).

At the critical frequency ω_D^* , the imaginary part of $\kappa_m(\mathcal{P}, \omega)$ rapidly increase, inducing a rapid increase of the phonon DOS. On the other hand, the periodic lattice exhibit a jump in DOS at $\omega_M^* = \sqrt{2\kappa_m(\mathcal{P}, 0)}$ corresponding to the minimum of the phonon dispersion relations at the edge of the 1BZ. At $\omega_S^* = \sqrt{3\kappa_m(\mathcal{P}, 0)}$ the DOS of the periodic lattice has a logarithmic singularity, corresponding to the saddle point of the phonon dispersion at $Q_S \simeq 4(3\kappa_m/2k)^{1/4}$ on the isostatic directions [9]. For the CPA effective medium, this singularity is totally

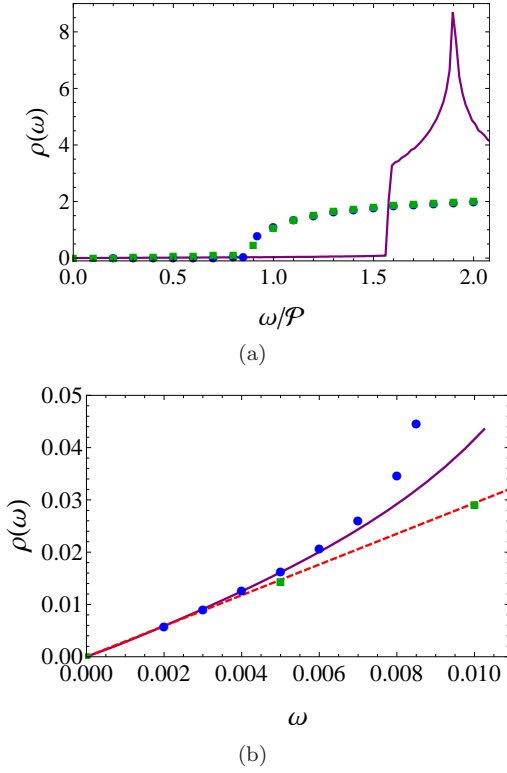


FIG. 7: (color online) (a) The phonon DOS at $\mathcal{P} = 0.01$ (blue circles) and $\mathcal{P} = 0.05$ (green squares) of the CPA effective medium and the pure kagome lattice with the NNN spring constant equal to the zero frequency effective medium value $\kappa_m(\mathcal{P}, \omega)$ for $\mathcal{P} = 0.01$ (purple line). The frequency is rescaled by \mathcal{P} . (b) The phonon DOS at small frequency for CPA effective medium (color scheme the same as in (a)). The Debye DOS defined in Eq. (46) is also shown as the red dashed line.

washed out due to the strong damping beyond ω_D^* , which is similar to the case of the square lattice [10].

D. Phonon scattering and the Ioffe-Regel limit

From the CPA solution at finite frequency, we identified a frequency scale ω_D^* beyond which phonon scattering rapidly increase. In this subsection we examine the scattering of phonons in more detail.

The scattering of the transverse phonons is characterized by the imaginary part of the phonon response function projected to the transverse direction $\text{Im}\chi_{TT}(\mathbf{q}, \omega)$. The phonon response function is defined as

$$\chi_{\mu,\nu}(\ell, t; \ell', t') \equiv \frac{\delta u_\mu(\ell, t)}{\delta F_\nu(\ell', t')}, \quad (47)$$

where t and t' label time, μ and ν label the basis defined in Eq. (12) of the 6-dimensional space of \mathbf{u} . This response function is related to the phonon Green's function through $\chi = -\mathbf{G}$. The imaginary part of the transverse component of this response function $\text{Im}\chi_{TT}(\mathbf{q}, \omega)$

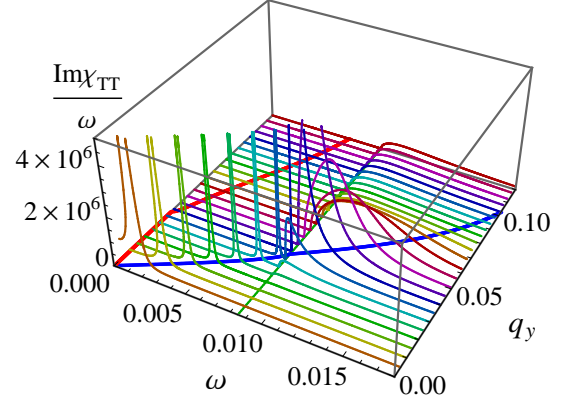


FIG. 8: (color online) Scattering of phonons characterized using the imaginary part of the transverse component of the phonon response function $\text{Im}\chi_{TT}(\mathbf{q}, \omega)$ as a function of ω for various values of q_y (we took $q_x = 0$ to follow the isostatic ΓM direction). The green line in the bottom plane marks ω_D^* , the blue and red lines marks the solution ω' and ω'' of the equation $\omega^2 - \omega_A(\mathbf{q}, \kappa_m(\mathcal{P}, \omega))^2 = 0$, which solves for the pole of the Green's function for the anomalous branch. The derivation of ω_A is shown in App. B 1.

characterizes the scattering of the transverse phonon by disorder. $\text{Im}\chi_{TT}(\mathbf{q}, \omega)$ is calculated for small momentum and frequency using the asymptotic CPA solution (42), and shown in Fig. 8. Also shown in the figure is the frequency at which the phonon Green's function of the anomalous branch has a complex pole, which is solved from the equation $\omega^2 - \omega_A(\mathbf{q}, \kappa_m(\mathcal{P}, \omega))^2 = 0$, which characterizes the dynamic dispersion relation. We use the form of ω_A as defined in App. B 1 for this calculation. It is clearly shown in the figure that below ω_D^* , the response function has Dirac-delta peaks at the frequencies determined by the transverse phonon dispersion relation $\omega = c_T q_y$. Above ω_D^* the imaginary part ω'' takes off, and the phonon peaks progressively broaden, showing that the transverse phonon is no longer a good eigenstate of the system. Furthermore, the hybridization of the transverse phonon and the rotational modes into the anomalous mode and the van Hove singularities in the density of states are washed out by the strong scattering. As a result, ω_O^* , ω_S^* , ω_M^* no longer play meaningful role in the dynamic response function.

The strength of the scattering can be characterized by the Ioffe-Regel (IR) limit, which states that the plane wave states are no longer well defined if the mean free path l_{mfp} is comparable to or less than the phonon wavelength λ . An equivalent condition is that the relaxation time becomes comparable to the period of the wave, i.e., $\omega'' \sim \omega'$. The solution for the positions of the complex poles of the Green's function of the anomalous branch $\omega^2 - \omega_A(\mathbf{q}, \kappa_m(\mathcal{P}, \omega))^2 = 0$ shows that the imaginary part ω'' becomes comparable to the real part ω' not far beyond ω_D^* and that $\omega_{\text{IR}}^* \sim \omega_D^* \sim \Delta z$. The associated

IR length scale can be derived from ω_D^* and c_T to be of order $l_{\text{IR}} \sim \sqrt{k/\kappa_m} \sim \Delta z^{-1}$.

This IR length scale differs from that in jammed solids, $l_d \sim \Delta z^{-1/2}$ as derived in Refs. [31, 32] (called l_s in Ref. [28]). This discrepancy can be attributed to the different scaling of the shear modulus G . In the kagome lattice, the shear modulus G is proportional to k and thus scales as Δz^0 , whereas in jammed solids $G \sim \Delta z$. Thus, the transverse speeds of sound scales as $(\Delta z)^0$ and $(\Delta z)^{1/2}$ in these two cases respectively. In both cases, the frequency beyond which plane wave states are strongly scattered is $\omega^* \sim \Delta z$. Therefore, the scattering length scale, c_T/ω^* are respectively $l^* \sim (\Delta z)^{-1}$ and $l_d \sim (\Delta z)^{-1/2}$ in the kagome lattice and jammed solids.

E. Comparison between different random nearly isostatic systems

Up to now, three examples of random nearly isostatic systems have been studied, including the random nearly isostatic square lattice, random nearly isostatic kagome lattice discussed in this Paper, and jammed solids near point J. In all cases, the characteristic frequency for the onset of the anomalous mode plateau $\omega^* \sim \Delta z$ and the isostatic length scale $l^* \sim (\Delta z)^{-1}$. On the other hand, the scaling of elastic moduli in the three cases are different because of different *network architecture*: in the square lattice $G \sim \kappa_m \sim (\Delta z)^2$ and $B \sim k \sim (\Delta z)^0$, in kagome lattice $G, B \sim k \sim (\Delta z)^0$, and in jammed solids $G \sim \Delta z$ and $B \sim k \sim (\Delta z)^0$ (a jump from zero to finite value at point J). As a result, the scattering length scales are also different. The square lattice is anisotropic, and we studied the scattering of the u_x vibrations along q_y direction and found that the scattering length corresponded to the point M in the first Brillouin zone, $q_y = \pi$, or $l_{x,\text{IR}} = a$. In kagome lattice $l_{\text{IR}} \sim c_T/\omega^* \sim (\Delta z)^{-1}$. In jammed solids, the IR length scale $l_d \sim c_T/\omega^* \sim (\Delta z)^{-1/2}$.

In Ref. [28], Wyart studied transport properties of amorphous solids modeled by an isotropic random network near its percolative rigidity threshold. In this system, both B and G vanish as Δz , and the crossover frequency between plane-wave and strongly scattered states is $\omega^* \sim \Delta z$. Both the longitudinal and transverse sound velocities scale as $(\Delta z)^{1/2}$, and the IR length $l_{\text{IR}} \sim c_{L,T}/\omega^*$ scales as $(\Delta z)^{-1/2}$ for both modes. The CPA self-consistency equation for low frequency in Ref. [28], Eq. (7), can be rewritten in the form

$$k_M^2 - (\Delta z)k_m + \omega^2 = 0, \quad (48)$$

by ignoring the ω^3 term which correspond to Rayleigh scattering in the second subequation. The solution to this equation

$$k_M = \frac{\Delta z}{2} \left(1 + \sqrt{1 - \frac{4\omega^2}{\Delta z^2}} \right), \quad (49)$$

has a form very similar to the that of the effective medium NNN spring constant κ_m in the kagome lattice as shown in Eq. (42). Although $k_M(\omega = 0) \sim \Delta z$ in the amorphous solid and $\kappa_M(\omega = 0) \sim (\Delta z)^2$ in the kagome lattice scale differently with Δz , the frequency dependence of $k_M(\omega)/k_M(\omega = 0)$ and $\kappa_M(\omega)/\kappa_M(\omega = 0)$ are almost identical: they are both of the form $a + b\sqrt{1 - (\omega/\omega_D^*)^2}$ where a and b are constants and $\omega_D \sim \Delta z$. The ω^3 term ignored in the above analysis leads to Rayleigh scattering and corresponds to the subdominant terms in f discussed in Sec. IV B. The difference between ω^3 in Ref. [28] and ω^2 for the kagome lattice is the spatial dimension.

To summarize, we examined the random nearly isostatic kagome lattice via the CPA, we obtained effective-medium NNN spring constant κ_m that scales with the occupancy probability $\mathcal{P} \sim \Delta z$ of the NNN bonds as \mathcal{P}^2 at small \mathcal{P} . Below the characteristic frequency $\omega_D^* \sim \mathcal{P}$, there is only weak damping of acoustic phonons arising from Rayleigh scattering, whereas above ω_D^* scattering increases rapidly and the system shows proximity to the IR limit. We compare the kagome lattice to other nearly isostatic systems including the square lattice, jammed solids near point J, and a model random isotropic network [28]. The characteristic frequency scale $\omega^* \sim \Delta z$, marking both the onset of the plateau of the anomalous modes and the strong scattering of plain wave states, is found to be a universal property of all of these systems. The elastic modulus G, B and thus the transport length scale depends on the *network architecture* and are not universal.

Acknowledgments—This work was supported in part by NSF-DMR-0804900.

Appendix A: The dynamical matrix of the kagome lattice

To construct the dynamical matrix of the kagome lattice, we use the form of the elastic energy given in Eq. (7). Because we consider the reference state of all bonds at their rest length, we have $f_b = 0$, thus there is only projection of u onto the direction along the bond. We first consider the case of simple lattice with one particle in each unit cell and rewrite Eq. (7) as

$$\begin{aligned} \Delta U &= \sum_b \frac{k_b}{2} [(\mathbf{u}_{\ell_1} - \mathbf{u}_{\ell_2}) \cdot \mathbf{e}_{\ell_1 \ell_2}]^2 \\ &= \sum_{\ell, \ell'} \sum_b \frac{k_b}{2} \mathbf{u}_{\ell} \cdot \mathbf{e}_{\ell_1 \ell_2} (\delta_{\ell, \ell_1} - \delta_{\ell, \ell_2}) \\ &\quad \times (\delta_{\ell', \ell_1} - \delta_{\ell', \ell_2}) \mathbf{e}_{\ell_1 \ell_2} \cdot \mathbf{u}_{\ell'}, \end{aligned} \quad (A1)$$

where ℓ_1, ℓ_2 labels the two particles connected by the bond b . Thus the dynamical matrix \mathbf{D} , as defined in Eq. (13), is given by

$$\begin{aligned} \mathbf{D}_{\ell, \ell'} &= \sum_b k_b \mathbf{e}_{\ell_1 \ell_2} (\delta_{\ell, \ell_1} - \delta_{\ell, \ell_2}) \\ &\quad \times (\delta_{\ell', \ell_1} - \delta_{\ell', \ell_2}) \mathbf{e}_{\ell_1 \ell_2}. \end{aligned} \quad (A2)$$

It is convenient to express the dynamical matrix in momentum space via the Fourier transform defined in Eq. (15)

$$\begin{aligned}
\mathbf{D}_{\mathbf{q},\mathbf{q}'} &= \sum_{\ell,\ell'} e^{-i\mathbf{q}\cdot\mathbf{r}_\ell + i\mathbf{q}'\cdot\mathbf{r}_{\ell'}} \mathbf{D}_{\ell,\ell'} \\
&= \sum_{\ell,\ell'} e^{-i\mathbf{q}\cdot\mathbf{r}_\ell + i\mathbf{q}'\cdot\mathbf{r}_{\ell'}} \sum_{\ell_1} \sum_{\ell_2}^{\prime} k_b \mathbf{e}_{\ell_1\ell_2} \\
&\quad \times (\delta_{\ell,\ell_1} - \delta_{\ell,\ell_2})(\delta_{\ell',\ell_1} - \delta_{\ell',\ell_2}) \mathbf{e}_{\ell_1\ell_2} \\
&= N\delta_{\mathbf{q},\mathbf{q}'} \sum_{\mathbf{b}} k_b (1 - e^{-i\mathbf{q}\cdot\mathbf{b}}) \\
&\quad \times (1 - e^{i\mathbf{q}\cdot\mathbf{b}}) \mathbf{e}_{\mathbf{b}} \mathbf{e}_{\mathbf{b}} \quad (\text{A3})
\end{aligned}$$

where the \prime above the summation of ℓ_2 denote a summation over particles connected to ℓ_1 , and $\mathbf{b} = \mathbf{r}_{\ell'} - \mathbf{r}_\ell$ represent the bonds connected to an arbitrary particle (note the difference from b in the previous equation, which represent all bonds in the system). One can define the dynamical matrix for translational invariant system as

$$\begin{aligned}
\mathbf{D}_{\mathbf{q},\mathbf{q}'} &= N\delta_{\mathbf{q},\mathbf{q}'} \mathbf{D}_{\mathbf{q}} \\
\mathbf{D}_{\mathbf{q}} &= \sum_{\mathbf{b}} k_b (1 - e^{-i\mathbf{q}\cdot\mathbf{b}})(1 - e^{i\mathbf{q}\cdot\mathbf{b}}) \mathbf{e}_{\mathbf{b}} \mathbf{e}_{\mathbf{b}} \\
&= \sum_m k_m \mathbf{B}_{m,\mathbf{q}} \mathbf{B}_{m,-\mathbf{q}}, \quad (\text{A4})
\end{aligned}$$

where the summation m is over bonds connected to an arbitrary particle, and the vector

$$\mathbf{B}_{m,\mathbf{q}} = (1 - e^{-i\mathbf{q}\cdot\mathbf{b}_m}) \mathbf{e}_{\mathbf{b}_m} \quad (\text{A5})$$

is a convenient way to express the dynamical matrix.

For the kagome lattice, which has three particles per unit cell, one need to modify the above construction of the dynamical matrix, and in the basis of

$$\mathbf{u}_\ell = (u_{\ell,1,x}, u_{\ell,1,y}, u_{\ell,2,x}, u_{\ell,2,y}, u_{\ell,3,x}, u_{\ell,3,y}), \quad (\text{A6})$$

with particles 1, 2, 3 labeled as in Fig. 2, the dynamical matrix can be expressed as

$$\begin{aligned}
\mathbf{D}_{\mathbf{q},\mathbf{q}'} &= N\delta_{\mathbf{q},\mathbf{q}'} \mathbf{D}_{\mathbf{q}}(k, \kappa) \\
\mathbf{D}_{\mathbf{q}}(k, \kappa) &= k \sum_{m \in NN} \mathbf{B}_{m,\mathbf{q}}^{NN} \mathbf{B}_{m,-\mathbf{q}}^{NN} \\
&\quad + \kappa \sum_{m \in NNN} \mathbf{B}_{m,\mathbf{q}}^{NNN} \mathbf{B}_{m,-\mathbf{q}}^{NNN}, \quad (\text{A7})
\end{aligned}$$

with the \mathbf{B} vectors for NN bonds for each unit cell (each

bond is counted once)

$$\begin{aligned}
\mathbf{B}_{1,\mathbf{q}}^{NN} &= \left(-\frac{1}{2}, -\frac{\sqrt{3}}{2}, \frac{1}{2}, \frac{\sqrt{3}}{2}, 0, 0 \right) \\
\mathbf{B}_{2,\mathbf{q}}^{NN} &= (0, 0, 1, 0, -1, 0) \\
\mathbf{B}_{3,\mathbf{q}}^{NN} &= \left(\frac{1}{2}, -\frac{\sqrt{3}}{2}, 0, 0, -\frac{1}{2}, \frac{\sqrt{3}}{2} \right) \\
\mathbf{B}_{4,\mathbf{q}}^{NN} &= \left(-\frac{1}{2}, -\frac{\sqrt{3}}{2}, \frac{1}{2} e^{-i(\frac{1}{2}q_x + \frac{\sqrt{3}}{2}q_y)}, \right. \\
&\quad \left. \frac{\sqrt{3}}{2} e^{-i(\frac{1}{2}q_x + \frac{\sqrt{3}}{2}q_y)}, 0, 0 \right) \\
\mathbf{B}_{5,\mathbf{q}}^{NN} &= (0, 0, -e^{-iq_x}, 0, 1, 0) \\
\mathbf{B}_{6,\mathbf{q}}^{NN} &= \left(\frac{1}{2}, -\frac{\sqrt{3}}{2}, 0, 0, -\frac{1}{2} e^{-i(-\frac{1}{2}q_x + \frac{\sqrt{3}}{2}q_y)}, \right. \\
&\quad \left. \frac{\sqrt{3}}{2} e^{-i(-\frac{1}{2}q_x + \frac{\sqrt{3}}{2}q_y)} \right), \quad (\text{A8})
\end{aligned}$$

and the \mathbf{B} vectors for NNN bonds for each unit cell

$$\begin{aligned}
\mathbf{B}_{1,\mathbf{q}}^{NNN} &= \left(\frac{\sqrt{3}}{2} e^{-iq_x}, \frac{1}{2} e^{-iq_x}, 0, 0, -\frac{\sqrt{3}}{2}, -\frac{1}{2} \right) \\
\mathbf{B}_{2,\mathbf{q}}^{NNN} &= (0, 0, 0, e^{-i(\frac{1}{2}q_x + \frac{\sqrt{3}}{2}q_y)}, 0, -1) \\
\mathbf{B}_{3,\mathbf{q}}^{NNN} &= \left(\frac{\sqrt{3}}{2}, \frac{1}{2}, 0, 0, -\frac{\sqrt{3}}{2} e^{-i(\frac{1}{2}q_x + \frac{\sqrt{3}}{2}q_y)}, \right. \\
&\quad \left. -\frac{1}{2} e^{-i(\frac{1}{2}q_x + \frac{\sqrt{3}}{2}q_y)} \right) \\
\mathbf{B}_{4,\mathbf{q}}^{NNN} &= \left(-\frac{\sqrt{3}}{2}, \frac{1}{2}, \frac{\sqrt{3}}{2} e^{-i(-\frac{1}{2}q_x + \frac{\sqrt{3}}{2}q_y)}, \right. \\
&\quad \left. -\frac{1}{2} e^{-i(-\frac{1}{2}q_x + \frac{\sqrt{3}}{2}q_y)}, 0, 0 \right) \\
\mathbf{B}_{5,\mathbf{q}}^{NNN} &= (0, 0, 0, 1, 0, -e^{-i(-\frac{1}{2}q_x + \frac{\sqrt{3}}{2}q_y)}) \\
\mathbf{B}_{6,\mathbf{q}}^{NNN} &= \left(-\frac{\sqrt{3}}{2} e^{iq_x}, \frac{1}{2} e^{iq_x}, \frac{\sqrt{3}}{2}, -\frac{1}{2}, 0, 0 \right). \quad (\text{A9})
\end{aligned}$$

Appendix B: Calculation of the asymptotic form of the $f(\kappa_m, \omega)$ function at small κ_m

1. The reduced dynamical matrix

To calculate the asymptotic form of $f(\kappa_m, \omega)$ we first simplify the problem by reduce the dynamical matrix into the space of its three low energy modes by integrating out its three high energy modes [9]. The resulting low-energy dynamical matrix is conveniently represented in the basis of longitudinal and transverse phonons and the rotational mode (mode ν_3)

$$(\nu'_1, \nu'_2, \nu'_3) = \left(\frac{q_x \nu_1 + q_y \nu_2}{|\mathbf{q}|}, \frac{-q_y \nu_1 + q_x \nu_2}{|\mathbf{q}|}, \nu_3 \right), \quad (\text{B1})$$

in which the dynamical matrix takes the form

$$\tilde{\mathbf{D}}^{(R)} = k \begin{pmatrix} \frac{3q^2}{16} & 0 & \frac{q^2}{16} \cos 3\theta \\ 0 & \frac{q^2}{16} & -\frac{q^2}{16} \sin 3\theta \\ \frac{q^2}{16} \cos 3\theta & -\frac{q^2}{16} \sin 3\theta & \frac{q^2}{16} + \frac{6\kappa_m}{k} \end{pmatrix}, \quad (\text{B2})$$

in leading order of small κ and quadratic order in q (the cross term of order $\kappa_m q^2$ is considered higher order and has been dropped).

Eigenmodes of the dynamical matrix are identified by diagonalizing $\tilde{\mathbf{D}}^{(R)}$. Strong mixing between the transverse mode and the rotational mode occurs along $q_x = 0$ (i.e., $\theta = 0$) and symmetry equivalent isostatic directions. The resulting two eigenvalues (by diagonalizing the lower right 2×2 block) are

$$\begin{aligned} \tilde{\omega}_A^2(q) &= \frac{q^2}{16} + 3\kappa_m - \sqrt{\left(\frac{q^2}{16}\right)^2 + (3\kappa_m)^2} \\ \tilde{\omega}_B^2(q) &= \frac{q^2}{16} + 3\kappa_m + \sqrt{\left(\frac{q^2}{16}\right)^2 + (3\kappa_m)^2}, \end{aligned} \quad (\text{B3})$$

2. Leading order divergence of $f(\kappa_m, \omega)$

The function $f(\kappa_m, \omega)$, as given in Eq. (33), can be analyzed using the simplified dynamical matrix (B2), which is the leading order form in small κ_m and q . Thus we can obtain an asymptotic analytical calculation of the integral f by projecting from the 6-dimensional basis in Eq. (12) onto the 3-dimensional basis in Eq. (B1) built from the three low energy modes of the system

$$\begin{aligned} f(\kappa_m, \omega) &= - \int_{1BZ} \frac{d^2 \mathbf{q}}{8\pi^2/\sqrt{3}} \mathbf{B}_{1,-\mathbf{q}}^{NNN} \cdot \mathbf{G}_{\mathbf{q}}(\omega) \cdot \mathbf{B}_{1,\mathbf{q}}^{NNN} \\ &\simeq - \int_{1BZ} \frac{d^2 \mathbf{q}}{8\pi^2/\sqrt{3}} \mathbf{B}_{1,-\mathbf{q}}^{NNN} \cdot \Theta^T \Theta \cdot \mathbf{G}_{\mathbf{q}}(\omega) \cdot \Theta^T \Theta \cdot \mathbf{B}_{1,\mathbf{q}}^{NNN}, \end{aligned} \quad (\text{B4})$$

where

$$\Theta = \begin{pmatrix} \frac{q_x}{\sqrt{3}q} & \frac{q_y}{\sqrt{3}q} & \frac{q_x}{\sqrt{3}q} & \frac{q_y}{\sqrt{3}q} & \frac{q_x}{\sqrt{3}q} & \frac{q_y}{\sqrt{3}q} \\ -\frac{q_y}{\sqrt{3}q} & \frac{q_x}{\sqrt{3}q} & -\frac{q_y}{\sqrt{3}q} & \frac{q_x}{\sqrt{3}q} & -\frac{q_y}{\sqrt{3}q} & \frac{q_x}{\sqrt{3}q} \\ -\frac{1}{\sqrt{3}} & 0 & \frac{1}{2\sqrt{3}} & -\frac{1}{2} & \frac{1}{2\sqrt{3}} & \frac{1}{2} \end{pmatrix}, \quad (\text{B5})$$

is the orthogonal transformation from the basis of $\mathbf{u}_\ell = (u_{\ell,1,x}, u_{\ell,1,y}, u_{\ell,2,x}, u_{\ell,2,y}, u_{\ell,3,x}, u_{\ell,3,y})$ to the basis (ν'_1, ν'_2, ν'_3) in Eq. (B1) with the longitudinal, transverse, and the rotational mode. In these new basis, the dynamical matrix is modified by integrating out the high energy modes and keeping to leading order in small κ_m and q , which lead to the simple form of Eq. (B2) [9], and thus the Green's function can be analyzed correspondingly. Note that we use the Green's function $\tilde{\mathbf{G}}_{\mathbf{q}}(\omega)$ calculated from the renormalized dynamical matrix (B2), so it is different from the bare value $\Theta \cdot \mathbf{G}_{\mathbf{q}}(\omega) \cdot \Theta^T$. The transformed the $\mathbf{B}_{1,\mathbf{q}}^{NNN}$ vector in the basis of (ν'_1, ν'_2, ν'_3) takes the form

$$\left(\frac{(e^{-iq_x} - 1)(3q_x + \sqrt{3}q_y)}{6|\mathbf{q}|}, \frac{(e^{-iq_x} - 1)(\sqrt{3}q_x - 3q_y)}{6|\mathbf{q}|}, -\frac{1}{2}(1 + e^{-iq_x}) \right). \quad (\text{B6})$$

The leading order term of this integral in small κ_m is from ν'_3 , the anomalous mode, which has a small frequency of order $\sqrt{\kappa_m}$ over the whole range of momentum from q_H to the edge of the Brillouin zone along the isostatic directions, and thus correspond to diverging contributions to the f integral in small κ_m .

For an approximation of the f integral at small κ_m , we use the dynamical matrix of the form (B2), which kept to leading order in κ_m and quadratic order in q . At small momentum, the dynamical matrix (B2) is diagonalized by the basis (ν'_1, ν'_2, ν'_3) , and the Green's function $\tilde{\mathbf{G}}_{\mathbf{q}}(\omega)$ takes the form of a diagonal matrix

$$\tilde{\mathbf{G}}_{\mathbf{q}}(\omega) = \text{Diag} \left(\frac{1}{\omega^2 - \frac{3q^2}{16}}, \frac{1}{\omega^2 - \frac{q^2}{16}}, \frac{1}{\omega^2 - 6\kappa_m - \frac{q^2}{16}} \right), \quad (\text{B7})$$

obtained from the quadratic order of the renormalized 3×3 matrix $\tilde{\mathbf{D}}^{(R)}$. The lower eigenvalue $\tilde{\omega}_A^2$ correspond to the *anomalous mode*, which is close to the transverse mode ν'_2 (which is simply ν_1 for $q_x = 0$ direction) for $q_y \ll q_H^* = 4\sqrt{3\kappa_m/k}$. For $q_y \gg q_H^*$ this anomalous mode corresponds to the linear combination of $(\nu'_2 - \nu'_3)/2$, which is actually the floppy mode of the kagome lattice in the $\kappa_m \rightarrow 0$ limit, in which $\tilde{\omega}_A \rightarrow 0$.

which is isotropic and valid for small momentum $|\mathbf{q}| < q_H^*$. Thus, the small momentum region contribute to f the following terms

$$f_{<}(\kappa_m, \omega) = - \int_{|\mathbf{q}| < q_H^*} \frac{dq_x dq_y}{8\pi^2/\sqrt{3}} \left\{ \frac{(1 - \cos q_x)(3q_x + \sqrt{3}q_y)^2}{18(q_x^2 + q_y^2)(\omega^2 - \frac{3(q_x^2 + q_y^2)}{16})} + \frac{(1 - \cos q_x)(\sqrt{3}q_x - 3q_y)^2}{18(q_x^2 + q_y^2)(\omega^2 - \frac{q_x^2 + q_y^2}{16})} + \frac{1 + \cos q_x}{2(\omega^2 - 6\kappa - \frac{q_x^2 + q_y^2}{16})} \right\} \quad (\text{B8})$$

At large momentum, the dynamical matrix can be diagonalized to leading order in κ_m in the basis $(\nu'_1, \frac{\nu'_2 + \nu'_3}{\sqrt{2}}, \frac{\nu'_2 - \nu'_3}{\sqrt{2}})$, in which $\mathbf{B}_{1,\mathbf{q}}$ takes the form

$$\begin{pmatrix} \frac{(e^{-iq_x} - 1)(3q_x + \sqrt{3}q_y)}{6|\mathbf{q}|}, \frac{(e^{-iq_x} - 1)(\sqrt{3}q_x - 3q_y)}{6\sqrt{2}|\mathbf{q}|} - \frac{1}{2\sqrt{2}}(1 + e^{-iq_x}), \\ \frac{(e^{-iq_x} - 1)(\sqrt{3}q_x - 3q_y)}{6\sqrt{2}|\mathbf{q}|} + \frac{1}{2\sqrt{2}}(1 + e^{-iq_x}) \end{pmatrix}, \quad (\text{B9})$$

and the Green's function $\mathbf{G}_{\mathbf{q}}(\omega)$ takes the form of a diagonal matrix

$$\tilde{\mathbf{G}}_{\mathbf{q}}(\omega) = \text{Diag} \left(\frac{1}{\omega^2 - \frac{3(q_x^2 + q_y^2)}{16}}, \frac{1}{\omega^2 - 6\kappa_m - \frac{q_x^2 + q_y^2}{16}}, \frac{1}{\omega^2 - \frac{1}{Q_M - Q_S} [Q_M \omega_S^2 - Q_S \omega_M^2 - q_y(\omega_S^2 - \omega_M^2)] - \frac{3q_x^2}{16}} \right), \quad (\text{B10})$$

which is for the direction of $q_x = 0$, and we have used the approximated form 20 of ω_A^2 , that represent the dispersion relation of the anomalous mode at large frequency, as depicted in Fig. 4. For this calculation we use the small κ_m values $(\omega_S^*)^2 = 3\kappa_m$ and $(\omega_M^*)^2 = 3\kappa_m$.

For the other two directions one should change the third term above from q_x^2 into the perpendicular direction of the two isostatic directions accordingly. Thus we need to divide the first Brillouin zone into 3 parts: $|\theta - \pi/2| < \pi/6$, $|\theta - \pi/6| < \pi/6$, and $|\theta - 5\pi/6| < \pi/6$, and integrate each of them out separately and then calculate the sum. Here we just do the $|\theta - \pi/2| < \pi/6$ part as an example, which uses the form of the Green's function in Eq. (B10). This part of the integral is

$$\begin{aligned} f_{>,\frac{\pi}{2}}(\kappa_m, \omega) = & - \frac{2}{8\pi^2/\sqrt{3}} \int_{q_H^*}^{\frac{2\pi}{\sqrt{3}}} dq_y \int_{-\frac{|q_y|}{\sqrt{3}}}^{\frac{|q_y|}{\sqrt{3}}} dq_x \left\{ \frac{(1 - \cos q_x)(3q_x + \sqrt{3}q_y)^2}{18(q_x^2 + q_y^2)(\omega^2 - \frac{3(q_x^2 + q_y^2)}{16})} \right. \\ & + \frac{(2 + \cos q_x)q_x^2 + \sqrt{3}(1 - \cos q_x)q_x q_y + 3q_y^2}{6(q_x^2 + q_y^2)(\omega^2 - 6\kappa_m - \frac{q_x^2 + q_y^2}{16})} \\ & \left. + \frac{(2 + \cos q_x)q_x^2 + \sqrt{3}(1 - \cos q_x)q_x q_y + 3q_y^2}{6(q_x^2 + q_y^2)(\omega^2 - \frac{Q_M \omega_S^2 - Q_S \omega_M^2 - q_y(\omega_S^2 - \omega_M^2)}{Q_M - Q_S} - \frac{3q_x^2}{16})} \right\}, \quad (\text{B11}) \end{aligned}$$

and the integral for the other two directions can be calculated similarly.

The leading order contribution to $f(\kappa_m, \omega)$ in small κ_m is from the third term in Eq. (B11), which represent the isostatic mode. We first consider the $\omega = 0$ case, for which the leading order term of $f(\kappa_m, \omega)$ is

$$\begin{aligned} f_{\frac{\pi}{2}, l.o.}(\kappa_m, 0) &= \frac{2}{8\pi^2/\sqrt{3}} \int_{q_H^*}^{\frac{2\pi}{\sqrt{3}}} dq_y \int_{-\frac{|q_y|}{\sqrt{3}}}^{\frac{|q_y|}{\sqrt{3}}} dq_x \frac{(2 + \cos q_x)q_x^2 + \sqrt{3}(1 - \cos q_x)q_x q_y + 3q_y^2}{6(q_x^2 + q_y^2) \left(\frac{Q_M \omega_S^2 - Q_S \omega_M^2 - q_y(\omega_S^2 - \omega_M^2)}{Q_M - Q_S} + \frac{3q_x^2}{16} \right)} \\ &\simeq \frac{2}{8\pi^2/\sqrt{3}} \int_{q_H^*}^{\frac{2\pi}{\sqrt{3}}} dq_y \frac{(2 + \cos q_x)q_x^2 + \sqrt{3}(1 - \cos q_x)q_x q_y + 3q_y^2}{6(q_x^2 + q_y^2)} \frac{\pi}{\sqrt{\frac{Q_M \omega_S^2 - Q_S \omega_M^2 - q_y(\omega_S^2 - \omega_M^2)}{Q_M - Q_S}}} \frac{4}{\sqrt{3}} \delta(q_x) \\ &\simeq \frac{2(1 - \sqrt{2/3})}{\sqrt{\kappa_m}}, \quad (\text{B12}) \end{aligned}$$

where we took the limit of $\kappa_m \rightarrow 0$ and make use of the identity $\lim_{a \rightarrow 0} \frac{1}{a^2 + x^2} = (\pi/a)\delta(x)$. Adding up the contribution from $\theta = \pi/6$ and $\theta = 5\pi/6$ part we have

$$f_{l.o.}(\kappa_m, 0) \simeq \frac{5(1 - \sqrt{2/3})}{\sqrt{\kappa_m}}. \quad (\text{B13})$$

Other terms in Eq. (B8) and (B11) contribute higher order terms in small κ_m , and is discussed in Sec. B 3.

In the case of $\omega > 0$, the leading order term can be calculated in a similar way

$$\begin{aligned}
f_{\frac{\pi}{2}, l.o.}(\kappa_m, 0) &= -\frac{2}{8\pi^2/\sqrt{3}} \int_{q_H^*}^{\frac{2\pi}{\sqrt{3}}} dq_y \int_{-\frac{|q_y|}{\sqrt{3}}}^{\frac{|q_y|}{\sqrt{3}}} dq_x \frac{(2 + \cos q_x)q_x^2 + \sqrt{3}(1 - \cos q_x)q_x q_y + 3q_y^2}{6(q_x^2 + q_y^2)(\omega^2 - \frac{Q_M \omega_S^2 - Q_S \omega_M^2 - q_y(\omega_S^2 - \omega_M^2)}{Q_M - Q_S} - \frac{3q_x^2}{16})} \\
&\simeq \frac{2}{8\pi^2/\sqrt{3}} \int_{q_H^*}^{\frac{2\pi}{\sqrt{3}}} dq_y \frac{1}{2} \frac{2\pi i(16/3)}{2(4/\sqrt{3})\sqrt{\omega^2 - \frac{Q_M \omega_S^2 - Q_S \omega_M^2 - q_y(\omega_S^2 - \omega_M^2)}{Q_M - Q_S}}} \\
&\simeq \frac{2}{\sqrt{3}\kappa_m} \left(\sqrt{3 - \frac{\omega^2}{\kappa_m}} - \sqrt{2 - \frac{\omega^2}{\kappa_m}} \right). \tag{B14}
\end{aligned}$$

The q_x integral can either be evaluated using the δ function trick by assuming an infinitesimal imaginary part of ω ($\omega \rightarrow \omega + i\delta$), or by extending the integral limit of q_x to $(-\infty, \infty)$ (because the integrand decays fast when q_x is large) and using contour integral. We also assumed that $|\sqrt{\frac{Q_M \omega_S^2 - Q_S \omega_M^2 - q_y(\omega_S^2 - \omega_M^2)}{Q_M - Q_S}} - \omega^2| \ll 1$ to make the simplification that $\cos q_x \simeq 1$. Adding up the contribution from $\theta = \pi/6$ and $\theta = 5\pi/6$ part we have

$$f_{l.o.}(\kappa_m, \omega) \simeq \frac{5}{\sqrt{3}\kappa_m} \left(\sqrt{3 - \frac{\omega^2}{\kappa_m}} - \sqrt{2 - \frac{\omega^2}{\kappa_m}} \right). \tag{B15}$$

Other terms in Eq. (B8) and (B11) contribute higher order terms in small κ_m , and is discussed in Sec. B 3.

3. Correction at small frequencies

To get the correction to the asymptotic solution of $\kappa_m(\mathcal{P}, \omega)$ as in (B15), in particular the small imaginary part rather than zero at small frequency, we calculate the imaginary part of f at small frequencies and solve for the correction to $\kappa_m(\mathcal{P}, \omega)$ perturbatively in the CPA equation.

Because we consider small frequencies $\omega^2 < \kappa_m$, the contribution is from the two acoustic modes, which are isotropic, and thus can be calculated as

$$\begin{aligned}
\text{Im} f_L &\simeq -\frac{2}{8\pi^2/\sqrt{3}} \int_0^{q_H^*} dq \int_0^{2\pi} d\theta q \text{Im} \left[\frac{q^2 \cos^2 \theta (3 \cos \theta + \sqrt{3} \sin \theta)^2}{18(\omega^2 - \frac{3}{16}q^2 + i\delta)} \right] \\
&\simeq \frac{20}{27} \omega^2, \tag{B16}
\end{aligned}$$

and

$$\begin{aligned}
\text{Im} f_T &\simeq -\frac{2}{8\pi^2/\sqrt{3}} \int_0^{q_H^*} dq \int_0^{2\pi} d\theta q \text{Im} \left[\frac{q^2 \cos^2 \theta (\sqrt{3} \cos \theta - 3 \sin \theta)^2}{18(\omega^2 - \frac{1}{16}q^2 + i\delta)} \right] \\
&\simeq 4\omega^2. \tag{B17}
\end{aligned}$$

Thus we have the correction to Eq. (B15) that is valid for small ω as

$$f(\kappa_m, \omega) = \frac{5}{\sqrt{3}\kappa_m} \left(\sqrt{3 - \frac{\omega^2}{\kappa_m}} - \sqrt{2 - \frac{\omega^2}{\kappa_m}} \right) + i \frac{128}{27} \omega^2. \tag{B18}$$

We then solve the leading order CPA equation in small κ_m nonaffine regime perturbatively using this corrected form of f at small ω , and get

$$\kappa_m(\mathcal{P}, \omega) = \kappa_m^{(0)} - \frac{256}{135(1 - \sqrt{2/3})} (\kappa_m^{(0)})^{3/2} i \omega^2, \tag{B19}$$

where $\kappa_m^{(0)}$ is the zeroth order solution (42). This correction is very small and can not be observed in our numerical solutions within precision.

-
- [1] J. C. Maxwell, *Phil. Mag.* **27**, 294 (1864).
 - [2] J. C. Phillips and M. F. Thorpe, *Solid State Commun.* **53**, 699 (1985).
 - [3] M. Thorpe, *J. Non-Cryst. Solids* **57**, 355 (1983).
 - [4] H. He and M. F. Thorpe, *Phys. Rev. Lett.* **54**, 2107 (1985).
 - [5] M. Wyart, L. E. Silbert, S. R. Nagel, and T. A. Witten, *Phys. Rev. E* **72**, 051306 (2005).
 - [6] M. Wyart, *Ann. Phys. Fr* **30**, 1 (2005).
 - [7] C. Heussinger and E. Frey, *Phys. Rev. Lett.* **97**, 105501 (2006).
 - [8] E. Huisman and T. C. Lubensky, Manuscript in preparation (2010).
 - [9] A. Souslov, A. J. Liu, and T. C. Lubensky, *Phys. Rev. Lett.* **103**, 205503 (2009).
 - [10] X. Mao, N. Xu, and T. C. Lubensky, *Phys. Rev. Lett.* **104**, 085504 (2010).
 - [11] V. Kapko, M. Treacy, M. Thorpe, and S. Guest, *Proc. R. Soc. A* **465**, 3517 (2009).
 - [12] C. Calladine, *Int. J. Solids Struct.* **14**, 161 (1978); S. Pellegrino and C. Calladine, *Int. J. Solids Struct.* **22**, 409 (1982).
 - [13] A. Souslov and T. C. Lubensky, Manuscript in preparation (2010).
 - [14] A. J. Liu and S. R. Nagel, *Nature* **396**, 21 (1998).
 - [15] P. Soven, *Phys. Rev.* **178**, 1136 (1969).
 - [16] S. Feng, M. F. Thorpe, and E. Garboczi, *Phys. Rev. B* **31**, 276 (1985).
 - [17] M. Thorpe, D. Jacobs, M. Chubynsky, and J. Phillips, *J. Non-Cryst. Solids* **266**, 859 (2000).
 - [18] D. J. Jacobs and M. F. Thorpe, *Phys. Rev. Lett.* **75**, 4051 (1995).
 - [19] M. Lax, *Rev. Mod. Phys.* **23**, 287 (1951).
 - [20] D. W. Taylor, *Phys. Rev.* **156**, 1017 (1967).
 - [21] R. J. Elliott, J. A. Krumhansl, and P. L. Leath, *Rev. Mod. Phys.* **46**, 465 (1974).
 - [22] S. Kirkpatrick, B. Velický, and H. Ehrenreich, *Phys. Rev. B* **1**, 3250 (1970).
 - [23] B. Budiansky, *J. Mech. Phys. Solids* **13**, 223 (1965).
 - [24] R. Hill, *J. Mech. Phys. Solids* **13**, 89 (1965).
 - [25] J. Gubernatis and J. Krumhansl, *J. of Appl. Phys.* **46**, 1875 (1975).
 - [26] P. G. de Gennes, *J. Phys. (Paris)* **37**, L (1976).
 - [27] E. J. Garboczi and M. F. Thorpe, *Phys. Rev. B* **31**, 7276 (1985).
 - [28] M. Wyart, *Europhys. Lett.* **89**, 64001 (2010).
 - [29] D. A. Head, A. J. Levine, and F. C. MacKintosh, *Phys. Rev. E* **72**, 061914 (2005).
 - [30] J. Wilhelm and E. Frey, *Phys. Rev. Lett.* **91**, 108103 (2003).
 - [31] N. Xu, V. Vitelli, M. Wyart, A. J. Liu, and S. R. Nagel, *Phys. Rev. Lett.* **102**, 038001 (2009).
 - [32] V. Vitelli, N. Xu, M. Wyart, A. J. Liu, and S. R. Nagel, *Phys. Rev. E* **81**, 021301 (2010).